TECHNICAL ANALYSIS REPORT No: 39/01

OCCURRENCE No: 200102263

REFERENCE No: BE/200100016

Examination of a Failed Compressor Blisk

General Electric CT7-9B Turboprop Engine

Saab Aircraft AB, SF-340B, VH-EKX

EXAMINATON OF A FAILED COMPRESSOR BLISK

General Electric CT7-9B Turboprop Engine
Saab Aircraft AB, SF340B, VH-EKX

1. FACTUAL INFORMATION

1.1 Introduction

On 23 May 2001, the take-off of a Saab 340 aircraft (VH-EKX) was discontinued as a result of the right engine failing. To investigate the event, the Australian Transport Safety Bureau carried out an examination of the first stage compressor blisk (bladed disk) from the affected engine. An earlier disassembly of the engine had found the component damaged by the partial loss of a single aerofoil (blade) section. The examination attributed the downstream damage within the engine to the effects of the released aerofoil section.

1.2 Component history

The blisk component was installed within a General Electric CT7-9B turboprop engine; serial number 785492. At the time of failure, the engine had operated for a total of 13,931 hours and 16,226 flight cycles. The engine manufacturer indicated that the failed stage-one blisk (p/no. 6055T83G14, s/no. GLHG4996) had been fitted to the engine since new. A supplied specification indicated that the blisk was produced as a forging from a proprietary precipitation hardening stainless steel alloy, similar to UNS S35500 (AM355).

1.3 Visual examination and fractography

1.3.1 General condition

The leading edges and tips of the blisk aerofoil sections had been damaged by multiple impacts (figures 1 & 2). The single fractured aerofoil had separated transversely at a mid-span location, around 29 millimetres above the root transition (figure 3). The rear edges of the blisk hub (adjacent to the stage two compressor wheel coupling) showed appreciable erosion around the full circumference (figure 4). Heat tinting and other evidence indicating rubbing contact against the housing was present over approximately two-thirds of the blisk circumference (figure 5). The forward (convex) surfaces of the aerofoils were coated with an oily, black deposit which increased in density toward the blade tips (figure 6). Beneath the deposit, the surfaces exhibited a bright, lustrous finish, typical of a metallic coating (figure 7). Conversely, the rearward (convex) surfaces exhibited appreciable erosion; being most pronounced toward and along the trailing edges (figure 8). The metallic coating appeared to have appreciably eroded away on this side.

Figure 1. Blisk front view – fractured blade is arrowed.

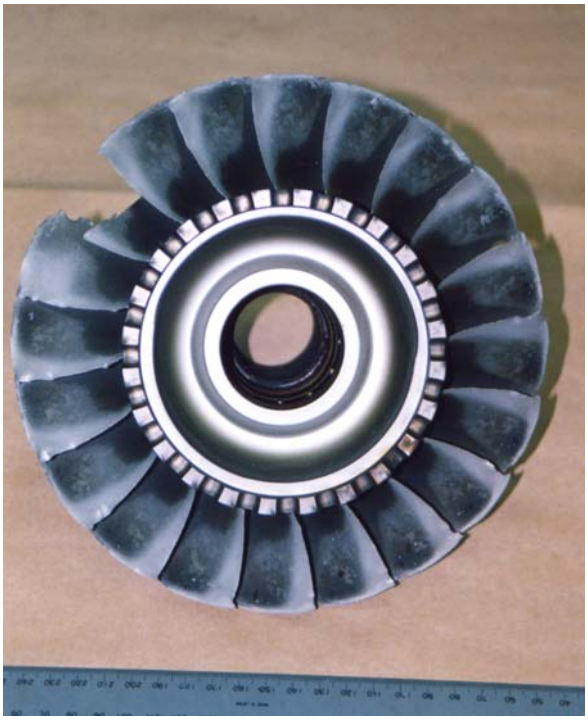

Figure 2. Blisk rear view.

Figure 3. Fractured blade and mechanical damage to other blades.

Figure 4. Erosion damage to rear edge of blisk hub.

Figure 5. Evidence of mechanical 'rub' on the rear edge of the blisk hub.

Figure 6. Dark deposit on the forward faces of the blisk aerofoils.

Figure 7. Forward (convex) aerofoil faces after cleaning. Bright finish is typical of a metallic coating.

Figure 8. Rear (concave) face of an aerofoil showing the typical eroded appearance.

1.3.2 Fracture surfaces

The aerofoil fracture extended over the full section width and was essentially straight from leading to trailing edges; a length of around 40 millimetres (figure 9). Just forward of the mid-chord position, a flat zone of brown stained fracture was present, forming semi-elliptical zones extending into the section from opposing locations on the external surfaces (figure 10). Beyond the stained area, a pattern of conchoidal crack progression marks extended further along the section (figure 11). A distinct step in the fracture path was present just rearward of the central stained zone; this also showed staining and crack progression marks (figure 12). When viewed in profile, the step feature was found to have formed from a second surface crack, immediately inward of the primary defect. Many other similar crack indications were also evident (figure 13).

Beyond the central stained and progressive cracking zones, the fracture presented features typical of ductile overload. Angular shear lips extended to the leading and trailing edges of the aerofoil (figure 14).

Figure 9. General view of the fractured blade lower section.

Figure 10. Closer view of the semi-elliptical stained regions at the mid-chord position.

Figure 11. Clear crack arrest marks extending out from the central stained region.

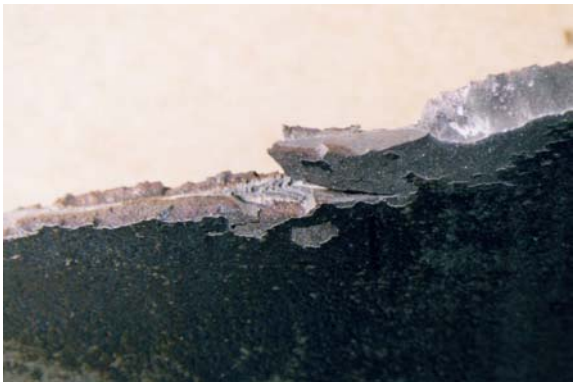

Figure 12. Progression of fracture on two adjacent planes, forming a step feature.

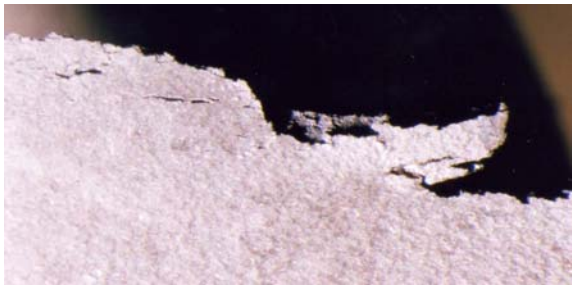

Figure 13. Many small fissures on the blade concave face, adjacent to the main fracture.

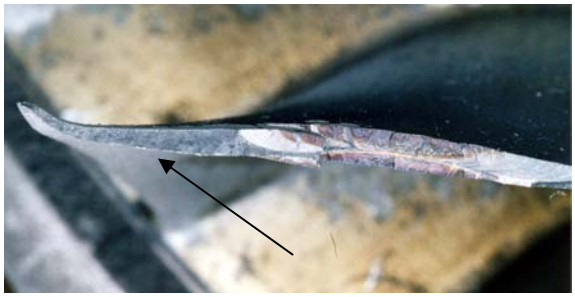

Figure 14. Area of ductile shear fracture (arrowed) behind the central fatigue zone.

1.3.3 Non-destructive inspection

Fluorescent liquid penetrant inspection of the full surface area of all remaining aerofoil sections and the blisk hub revealed no discontinuities or defect indications of any nature. Detailed inspection of the aerofoil mid-span positions on both surfaces found no indications of any further cracking or pre-existing defects.

1.3.4 Electron microscopy

Under examination using the scanning electron microscope, the aerofoil fracture clearly presented the two central zones observed visually (attachment A). The opposing semi-elliptical regions displayed multiple ratchet or step marks extending inward from the surfaces on both sides (figure 15). The marks were indicative of fatigue crack initiation sites. The actions of fatigue cracking were also indicated by the presence of conchoidal crack arrest marks extending away from the inner stained zones (figure 16). Close study revealed around nine such marks between the boundary of the stained region and the commencement of the ductile shear region. Due to the degree of oxidation and staining of the central zone, it was not possible to characterise the fracture features in that area. The transitional regions exhibited clear evidence of a progressive cracking mechanism, changing at the extremities to the dimpled and undulating surfaces that are typical of ductile tensile overload (figure 17).

Examination of the aerofoil surfaces adjacent to the fracture found many small fissures, some of which had partially opened (figure 18). Remnants of blade coating were also apparent, although much of the material had spalled away from the area adjacent to and along the fracture path.

The examination did not find any evidence of material or manufacturing defects associated with the fracture or the related cracking.

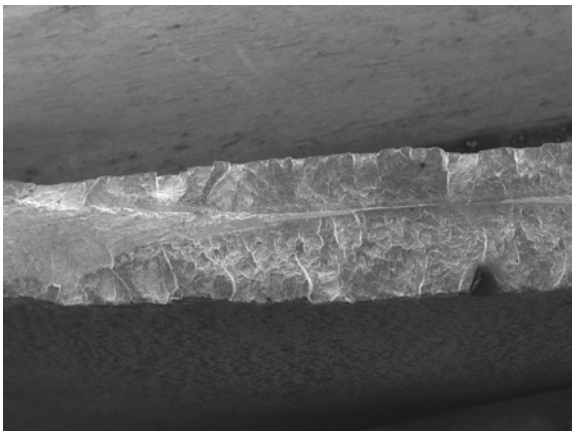

Figure 15. Low magnification SEM view of the central stained area of fracture.

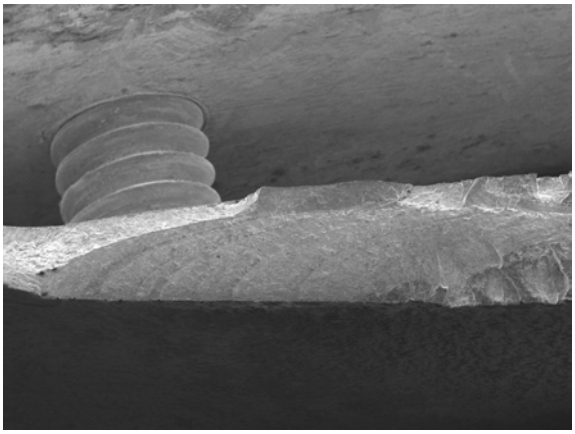

Figure 16. Area of crack arrest marks.

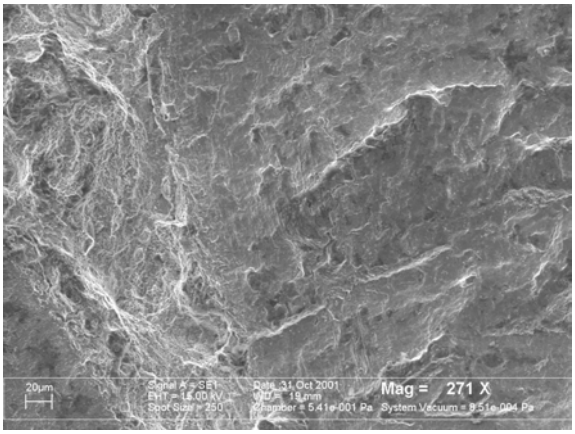

Figure 17. Higher magnification view of the transition between fatigue and overload fracture regions.

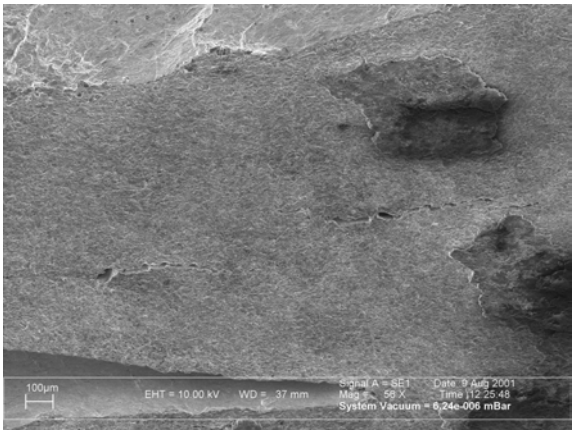

Figure 18. Fissures observed on the blade surface, adjacent to the primary fracture.

1.4 Chemical analysis

Analysis of a small sample of the blisk alloy returned the following results.

Fe	C	Mn	Si	S	P	Ni	Cr	Mo	Cu	Nb	Ti	Al
Bal	.12	.90	.50	.010	.028	3.9	14.6	2.7	.08	<.05	<.05	<.05

As such, the alloy generally complied with the specification for the blisk alloy, with the exception of the Nickel content (0.1% low) and Chromium content (0.4% low). In view of possible effects on material performance, these discrepancies were considered minor.

1.5 Metallographic examination

A suitably prepared metallographic section was taken transversely through the fracture (radially along the aerofoil axis), intersecting the central stained region. Examination of the section in the unetched condition revealed many shallow cracks extending into the section from both surfaces (figure 19). The cracks extended to a maximum depth of 370µm and several contained a dense product toward the surface (figure 20). Re-examination of the specimen after etching showed the primary fracture and crack morphology to be transgranular (typical of fatigue cracking) and did not exhibit any association with a material or microstructural anomaly. The general microstructure was mostly martensitic throughout with a preferred orientation that was typical of the forged production of the blisk (figure 21). Intermittent bands with an increased proportion of retained austenite were evident throughout the microstructure.

To further evaluate the condition of the blisk, a second blade was removed from the hub and sectioned in the same longitudinal manner as the first (figure 22). Subsequent examination revealed at least eight shallow surface cracks extending into the section from the convex surface. The cracks were measured at between 39 and 70µm spacing and extended to a maximum depth of 190µm. Cracking was not observed on the concave side.

The metallographic sections also confirmed the presence of a metallic surface coating over the aerofoil surfaces. Typically, the coating measured between 20 - 25µm on the convex sides and 0 - 20µm on the concave sides as a result of the abrasion damage noted visually.

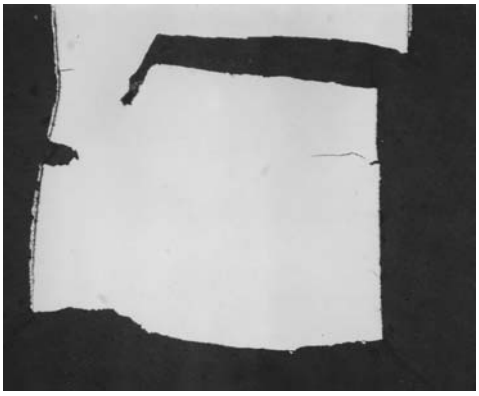

Figure 19. Section through the aerofoil showing the primary fracture and secondary cracking. X40

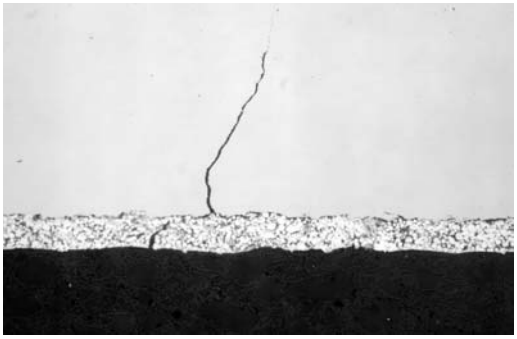

Figure 20. Larger secondary crack with notable oxide contents X320

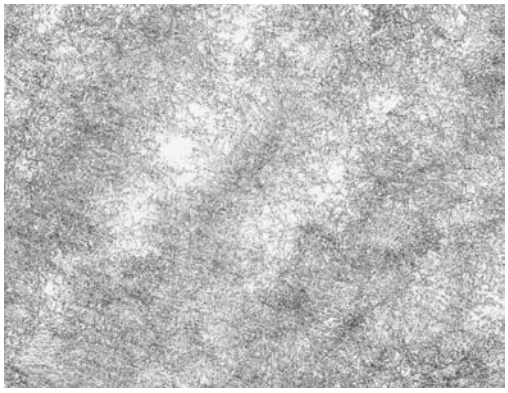

Figure 21. Martensite / retained austenite aerofoil microstructure.

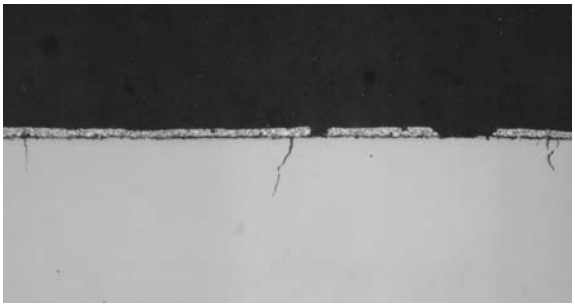

Figure 22. Cracking found in adjacent aerofoil. X80

1.6 EDS analysis

Energy dispersive x-ray analysis of the contents of some of the shallow secondary cracks produced characteristic spectra with major peaks for oxygen, iron and chromium (figure 23). Minor peaks for nickel and molybdenum were also identified. All of the elements were associated with the blisk alloy or with associated corrosion products.

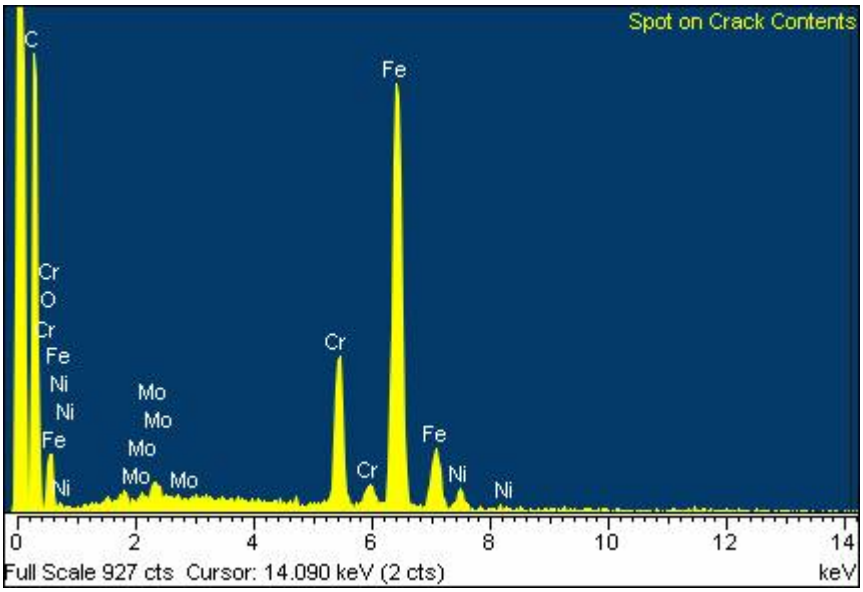

Figure 22. EDS spectra of the crack contents.

1.7 Hardness tests

Vickers hardness tests conducted on the fractured aerofoil cross-sections returned results of 362 – 375 HV_{30} (approximately 344 – 357 HB), meeting the specification requirements for the AM355 alloy.

2. ANALYSIS

The examination carried out on the first stage compressor blisk found no indications that the failure resulted from a deficiency within the material or production of the component. All examined aspects of the blisk's manufacture were consistent with the specifications provided and no anomalous features were found.

Fracture of the blisk aerofoil section was shown by visual evidence to have occurred as a result of fatigue cracking that initiated from corresponding transverse mid-span locations on both sides of the aerofoil. Such initiation was an indication of vibratory bending of the aerofoils. The zonal nature of the fracture typified the two-stage propagation of the fatigue cracking and indicated that the initial development and growth had been slow, extending over numerous hours and flight cycles. At approximately nine cycles before failure the cracking began to advance much more rapidly, possibly because of an increase in the engine vibration levels or the due to the inherent fracture characteristics of the material. During engine operation at take-off power on the final cycle, the crack grew to critical size and final overload fracture of the remaining section allowed the release of the outer aerofoil section.

Further strong evidence of the effects of vibratory bending of the blisk aerofoils was found in the form of many shallow cracks both adjacent to the primary fracture and in an adjacent aerofoil that had not failed. The cracks (maximum depth ~0.4 millimetres) were not detected by non-destructive examination. Many of the defects contained oxide and corrosion products, attesting to their slow growth and existence before the aerofoil failure event.

3. FINDINGS

- No anomalies were found within the blisk material.
- Failure of the aerofoil section resulted from the growth of reversed bending fatigue cracking at the mid-span location.
- Vibratory loading, exciting blade resonance was the principal source of stress driving the fatigue cracking.

Attachment A. Montage image of the full region of aerofoil fatigue fracture.